

INVITED PAPER

Design and modeling of a transistor vertical-cavity surface-emitting laser

Wei Shi · Behnam Faraji · Mark Greenberg · Jesper Berggren · Yu Xiang · Mattias Hammar · Michel Lestrade · Zhi-Qiang Li · Z. M. Simon Li · Lukas Chrostowski

Received: Oct. 4, 2010 / Accepted: Jan. 25, 2011

Abstract A multiple quantum well (MQW) transistor vertical-cavity surface-emitting laser (T-VCSEL) is designed and numerically modeled. The important physical models and parameters are discussed and validated by modeling a conventional VCSEL and comparing the results with the experiment. The quantum capture/escape process is simulated using the quantum-trap model and shows a significant effect on the electrical output of the T-VCSEL. The parameters extracted from the numerical simulation are imported into the analytic modeling to predict the frequency response and simulate the large-signal modulation up to 40 Gbps.

Keywords Transistor laser · VCSEL · Numerical modeling · Quantum-trap model · Direct modulation

1 Introduction

While most semiconductor lasers are diode structures, transistor lasers [1] are attracting much attention for their potential for high-frequency operation [2] and unique carrier dynamics [3]. Different from monolithically integrating a transistor and a laser diode, either in-plane [4] or vertically [5], where the transistor performs as the electrical driver of the laser, transistor lasers use the base

The UBC authors acknowledge support from the National Science and Engineering Research Council and the British Columbia Innovation Council.

Wei Shi, Behnam Faraji, Mark Greenberg, and Lukas Chrostowski*
 Department of Electrical and Computer Engineering, The University of British Columbia, Vancouver, BC, Canada * E-mail: lukasc@ece.ubc.ca

Jesper Berggren, Yu Xiang, and Mattias Hammar
 School of Information and Communication Technology (ICT), The Royal Institute of Technology (KTH), 16440 Kista, Sweden

Michel Lestrade, Zhi-qiang Li, and Z. M. Simon Li Crosslight Software Inc., 121-3989 Henning Dr. Burnaby, BC , V5C 6P8 Canada

recombination to provide stimulated emission. Early works on transistor lasers include a conceptual proposal of quantum well (QW) transistor lasers [6] and experimental demonstration of a laser transistor [7] that could function as a laser and a transistor in separate states. The recently developed QW transistor laser [1] has two independent control signals and can simultaneously output an electrical signal and an optical signal. This makes possible a simpler method of implementing feedback operation [8], a unique voltage-controlled mode [9], and a new optoelectronic integration scheme. Compared with edge-emitting lasers, vertical-cavity surface-emitting lasers (VCSELs) have many attractive features [10] such as low power consumption, large-scale 2D array fabrication, on-wafer testing, single longitudinal mode operation, and a narrow circular beam. Integrating a heterojunction bipolar transistor (HBT) structure into a vertical cavity, transistor VCSELs (T-VCSELs) [9] could combine the optoelectronic properties of the transistor laser with the advantages of VCSELs.

In this work, we design and model a multiple QW (MQW) T-VCSEL self-consistently. The important parameters are calibrated by matching the simulation to the experiment of a conventional VCSEL. We link the numerical model with our previously developed analytic model [11], using the quantum-trap model, to predict its frequency response and large-signal-modulation performance under different transistor bias configurations.

2 Design

The T-VCSEL, as shown in Fig. 1, has an Npn $\text{In}_{0.49}\text{Ga}_{0.51}\text{P}/\text{GaAs}$ HBT structure. The bottom and top distributed Bragg reflectors (DBRs) consist of 36 pairs and 24 pairs of $\text{Al}_{0.85}\text{Ga}_{0.15}\text{As}/\text{GaAs}$, respectively. The base region plays a critical role in determining the electrical and optical performance of a transistor laser [12]. In this design, we use an asymmetric base doping profile where the whole base region is composed of (from bottom to top) a 15 nm heavily doped ($1 \times 10^{19} \text{ cm}^{-3}$) layer, a 30 nm doping grading layer, three intrinsic $\text{In}_{0.17}\text{Ga}_{0.83}\text{As}/\text{GaAs}$ QWs, another 30 nm doping grading layer, and a 40 nm heavily doped ($1 \times 10^{19} \text{ cm}^{-3}$) base-contact layer. The heavily doped layers are aligned with the nodes of the longitudinal standing wave (as shown in the inset of Fig. 1) in the vertical cavity to reduce the optical absorption. A 6 μm -diameter oxide aperture is used for electrical and optical confinement.

3 Numerical modeling

To investigate the physics and performance of the T-VCSEL, we have used PICS3D, an advanced numerical simulation software [13], that solves the electrical and optical models numerically and self-consistently. The carrier transport is described based on the classic drift-diffusion model [14], with the thermionic-emission model [14] used at the heterojunctions. Lateral optical modes are calculated by the effective-index method [15]. In the strained QWs,

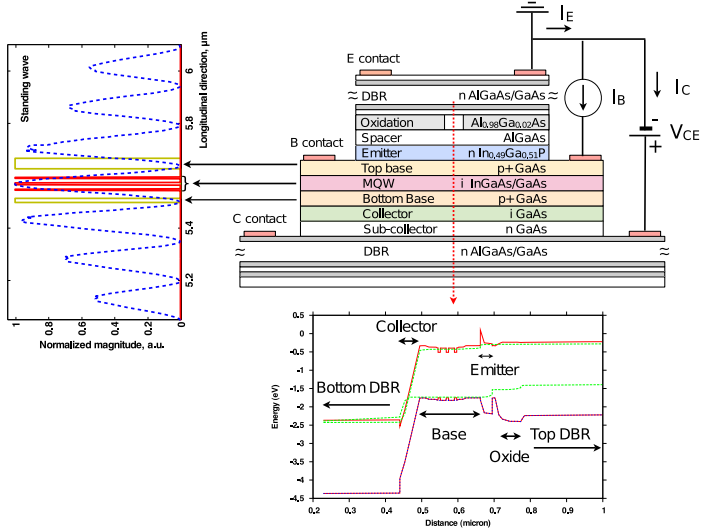


Fig. 1 Structure of the T-VCSEL with the DC bias configuration labeled. The insets show the standing wave (left) in the cavity with the positions of the QWs and heavily doped layers labeled and the typical band diagram (bottom) above threshold at the device center.

the conduction bands are assumed to be parabolic, and the valence bands are calculated by the 6×6 kp method for the valance-band mixing [16]. The important parameters for QWs are carefully calibrated to match the measured photoluminescence (PL): while the reported values of the band-edge offset for strained InGaAs/GaAs QWs have a big spread [17], it is assumed to be $\Delta E_c : \Delta E_v : 0.8 : 0.2$ [18]; a scattering time of 85 fs is used in Lorentz broadening; bandgap renormalization is considered as a function of the local carrier density of electrons (n) and holes (p): $\Delta E_g = 3 \times 10^{-10} \text{ eV/m} \cdot (n/2 + p/2)^{1/3}$. With Coulomb enhancement [19] included in calculating the optical gain and spontaneous emission, good agreement is achieved for the PL spectrum, as shown in Fig. 2 (a). The optical loss due to the free-carrier and intervalence-band absorption is calculated by $\alpha = k_n \cdot n + k_p \cdot p$ with $k_n = 3 \times 10^{-18} \text{ cm}^2$ and $k_p = 6 \times 10^{-18} \text{ cm}^2$ for the passive layers [20] and $k_n = 6 \times 10^{-18} \text{ cm}^2$ and $k_p = 14 \times 10^{-18} \text{ cm}^2$ for the QWs [21]. The Auger recombination is calculated by $R_{aug} = C_p \cdot n \cdot p^2$ by assuming that the CHHS Auger process dominates [22]. The Auger coefficient C_p is assumed to be $6.5 \times 10^{-30} \text{ cm}^6 \cdot \text{s}^{-1}$ for the passive layers [23] and $1 \times 10^{-29} \text{ cm}^6 \cdot \text{s}^{-1}$ for the QWs [24]. To verify the models and determine the material parameters, we have fabricated and simulated a conventional oxide-confined VCSEL that has the same QW structure as the designed T-VCSEL, taking self-heating into consideration. The power-law model [25] is used for AlGaAs thermal conductivity. The thermal conductivity (κ) of the AlGaAs/GaAs DBRs as a function of temperature (T) is given by $C_{sct}^\kappa \cdot (\kappa_{AlGaAs}(T)/2 + \kappa_{GaAs}(T)/2)$ where C_{sct}^κ is used to describe the effect of phonon scattering [26] due to the DBR interfaces and is tuned to be 0.5 for the lateral direction and 0.4 for the vertical direction. The carrier mobil-

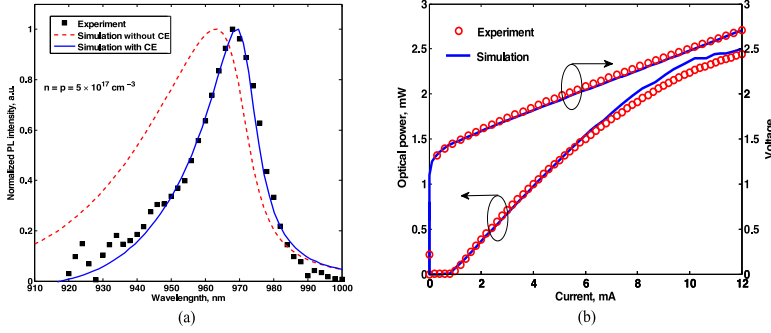


Fig. 2 Simulation vs. measurement of an InGaAs MQW VCSEL: (a) PL spectrum, with and without Coulomb enhancement (CE) in the simulation; (b) L - I - V curves.

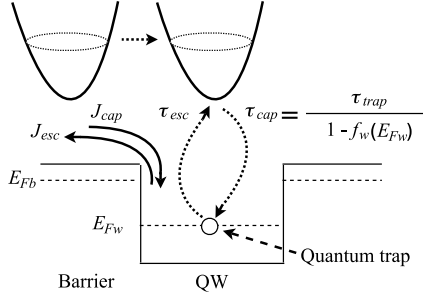


Fig. 3 Illustration of the QW capture/escape process and the quantum-trap model.

ity is also affected by the phonon scattering and 75-percent reduction of the average mobility of AlGaAs and GaAs for the DBRs gives a good agreement with measured LIV curves, as demonstrated in Fig. 2 (b). Thermal effect is not considered in the T-VCSEL modeling.

The QW capture/escape process has a significant influence on the frequency response of QW diode lasers [27] as well as of transistor lasers [11]. In this work, this process is described by a quantum-trap model in which the QWs are treated as carrier traps with trapping rates determined by phonon scattering theory [28]. The capture current (J_{cap}) and escape current (J_{esc}) of electrons (the minority carriers in the base) are given by

$$\begin{aligned} J_{cap}(E_{F_b}, E_{F_w}) &= \frac{1}{\tau_{cap}} \cdot d_w \cdot n_b(E_{F_b}) \\ &= \frac{1}{\tau_{trap}} \cdot d_w \cdot n_b(E_{F_b}) \cdot [1 - f_w(E_{F_w})] \end{aligned} \quad (1)$$

$$J_{esc}(E_{F_w}) = \frac{1}{\tau_{esc}} \cdot d_w \cdot n_w(E_{F_w}) \quad (2)$$

where τ_{cap} , τ_{trap} , and τ_{esc} are capture time, trapping time, and escape time, respectively; d_w is the QW thickness; n , E_F , and f represent carrier density, quasi-Fermi level, and occupancy, respectively, with the subscripts w indicating

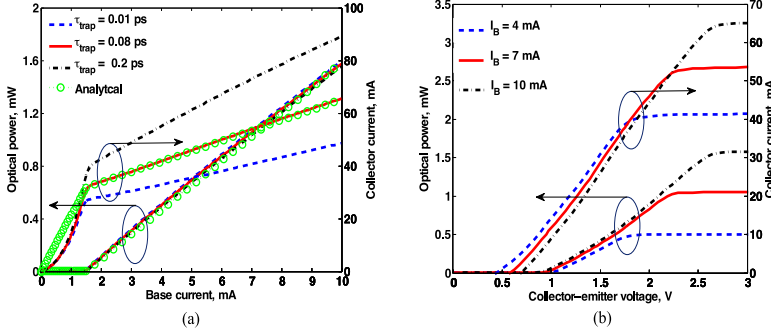


Fig. 4 (a) Optical power and I_C as a function of I_B at $V_{CE} = 4$ V with varied τ_{trap} ; (b) Optical power and I_C as a function of V_{CE} with varied I_B .

“well” and b “barrier”. From Eq. 1 we see that τ_{cap} can be determined from τ_{trap} based on the Fermi-Dirac distribution. In addition, τ_{esc} can be calculated by τ_{cap} in the quasi-equilibrium condition in which E_{F_b} is assumed to be equal to E_{F_w} and hence $J_{esc} = J_{cap}$. Therefore, from Eq. 1 and 2 we can find τ_{esc} :

$$\frac{1}{\tau_{esc}} = \frac{1}{\tau_{trap}} \cdot \frac{n_b(E_{F_w})}{n_w(E_{F_w})} \cdot [1 - f_w(E_{F_w})] \quad (3)$$

4 DC performance

In the active state of transistor operation, the emitter-base junction is forward biased and the collector-base junction is reversed biased, which is evident in the band diagram (Fig. 1). Fig. 4 (a) shows the simulated electrical output (collector current I_C) and optical output as functions of the input signal (base current I_B). The electrical gain drops suddenly (from 21.2 to 3.9 for $\tau_{trap} = 0.08$ ps) at threshold (1.5 mA) due to the stimulated emission. We notice that while the L-I curves are almost unaffected by the trapping time, the collector current is very sensitive to the capture/escape process. This is because the stimulated emission is dominated by the hole current injected into the base, however, the electrons can either be recombined with the holes in the optical collector (i.e. QWs) or leave the transistor via the electrical collector. In the following simulation, we use $\tau_{trap} = 0.08$ ps that corresponds to a capture time of ~ 1 ps at threshold [11]. Due to the three-port operation and device geometry, the optical power of a T-VCSEL is controlled both by the base current (which is determined by the base recombinations) and the collector-emitter voltage V_{CE} (that controls the effective current injected into the optical cavity) [9]. As shown in Fig. 4 (b), the optical output follows the same trend as the collector current, which means that we can potentially monitor the optical performance by the electrical output. This voltage-controlled operation may find applications in optical communications and signal processing [29].

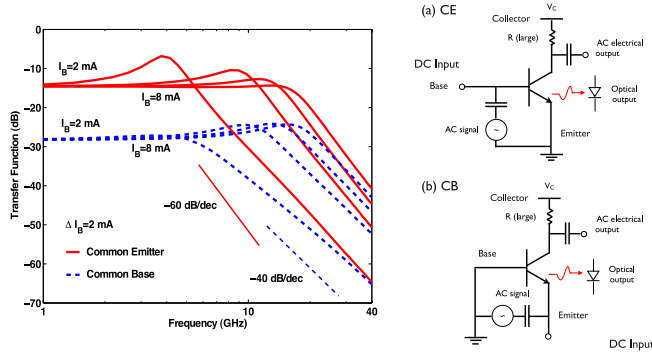


Fig. 5 Frequency responses of the small-signal modulation of the T-VCSEL in the CE and CB configurations. The insets show (a) the CE configuration and (b) the CB configuration.

5 Modulation response

Several analytic models, including the charge-control model [2] and the carrier-transport model that considers the quantum capture/escape process [11] have been developed. These models have been used to investigate the transistor lasers' frequency response [2, 11] and large-signal modulation [30, 31]. Here we use the model developed in [11] and solve the equations numerically by the finite difference method [32]. Using the parameters extracted from the numerical modeling by PICS3D, the analytic model matches well the DC results from the numerical simulation, as shown in Fig. 4 (a). Knowing the minority carrier distribution, we can study the T-VCSEL's modulation behavior under different configurations, i.e., common-emitter (CE) or common-base (CB). Fig. 5 shows the frequency responses of the T-VCSEL in both configurations. We can see that while the CE configuration has the same response as normal laser diodes (as shown in [11]), the CB configuration demonstrates a -40 dB/dec decay after relaxation oscillation and a bandwidth enhancement, albeit, a reduction of the DC response due to the transistor current gain [11]. For the large-signal modulation, we report the eye-diagrams for both configurations. Figs. 6 (a)-(c) show the eye-diagrams of the T-VCSEL, in the CB configuration, directly modulated at 10, 20, and 40 Gbps, respectively. Figs. 6 (e)-(f) are for the CE configuration. We can see that while the "eye" of the CE configuration starts closing at 20 Gbps, the CB configuration has an open eye-diagram up to 40 Gbps due to a larger bandwidth.

6 Conclusions

We have demonstrated the design and modeling of an InGaAs MQW T-VCSEL, a vertical-cavity laser with an extra electrical output coupled to its optical output. The model has been verified by modeling a conventional VCSEL and matching the simulation results with experiments. It has been shown that the quantum capture/escape process (described by a quantum-trap model

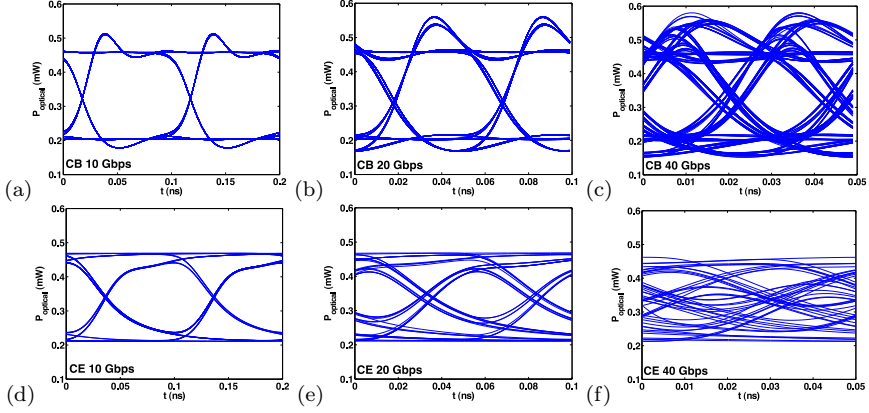


Fig. 6 Eye-diagrams of the digital modulation of the T-VCSEL: (a), (b), and (c) are for the CB configuration at a bit-rate of 10, 20, and 40 Gbps, respectively, where I_B is varied from 2.6 mA to 5 mA; (d), (e), and (f) are for the CE configuration at a bit-rate of 10, 20, and 40 Gbps, respectively, where I_E is varied from 42 mA to 53 mA. The modulation currents are chosen so that the output optical powers are the same for both configurations.

in this work) in the base of the T-VCSEL significantly affects its electrical output and, although less important for its optical DC performance, needs to be carefully treated for calculating its optical frequency response as it is highly related to the transistor's electrical gain. Our simulation has predicted a bandwidth enhancement and better large-signal performance of the T-VCSEL in the CB configuration. With a compact size, large-scale-integration capacity, a high bandwidth, and flexible three-port operation, the T-VCSEL should find novel applications in optical communications, optoelectronic data processing, and optical interconnects.

References

1. M. Feng, J. N. Holonyak, G. Walter, and R. Chan, "Room temperature continuous wave operation of a heterojunction bipolar transistor laser," *Appl. Phys. Lett.* **87**, p. 131103, 2005.
2. H. W. Then, M. Feng, and J. N. Holonyak, "Microwave circuit model for the three-port transistor laser," *Appl. Phys. Lett.* **107**, p. 094509, 2010.
3. B. Faraji, W. Shi, D. L. Pulfrey, and L. Chrostowski, "Common-emitter and common-base small-signal operation of the transistor laser," *Appl. Phys. Lett.* **93**, p. 143503, 2008.
4. J. Katz, N. Bar-Chaim, P. C. Chen, S. Margalit, I. Ury, D. Wilt, M. Yust, and A. Yariv, "A monolithic integration of GaAs/GaAlAs bipolar transistor and heterostructure laser," *Appl. Phys. Lett.* **37**, pp. 211–213, 1980.
5. T. R. Chen, K. Utaka, and Y. H. Z. Y. L. A. Yariv, "Vertical integration of an InGaAsP/InP heterojunction bipolar transistor and a double heterostructure laser," *Appl. Phys. Lett.* **50**, pp. 874–876, 1987.
6. F. Jain, C. Chung, R. LaComb, and M. Gokhale, "Resonant tunneling transistor lasers: A new approach to obtain multi-state switching and bistable operation," *Intl. J. Infrared and Millimeter Waves* **14**, pp. 1311–1322, 1993.
7. Y. Mori, J. Shibata, Y. Sasai, H. Serizawa, and T. Kaijiwara, "Operation principle of the InGaAsP/InP laser transistor," *Appl. Phys. Lett.* **47**, pp. 649–651, 1985.

8. B. Faraji, N. A. F. Jaeger, and L. Chrostowski, "Modelling the effect of the feedback on the small signal modulation of the transistor laser," in *23rd Annual Meeting of the IEEE Photonics Society*, p. WX4, (Denver, CO, USA), 11 2010.
9. W. Shi, L. Chrostowski, and B. Faraji, "Numerical study of the optical saturation and voltage control of a transistor vertical cavity surface emitting laser," *IEEE Photonics Technology Letters*, **20**, pp. 2141–2143, 2008.
10. I. Koyama, "Recent advances of VCSEL photonics," *IEEE J. Lightwaves* **24**, pp. 4502–4513, 2006.
11. B. Faraji, W. Shi, D. L. Pulfrey, and L. Chrostowski, "Analytical modeling of the transistor laser," *IEEE J. Quantum Electron.* **15**, pp. 594–603, 2009.
12. Z. Duan, W. Shi, L. Chrostowski, X. Huang, N. Zhou, and G. Chai, "Design and epitaxy of 1.5 μm InGaAsP-InP mqw material for a transistor laser," *Optics Express* **18**, pp. 1501–1509, 2010.
13. *Crosslight Device Simulation Software – A General Description*, Crosslight Software Inc., 2005.
14. S. M. Sze, *Physics of Semiconductor Devices*, Wiley-Interscience; 2nd Edition, New York, 1981.
15. G. R. Hadley, K. L. Lear, M. E. Warren, K. D. Choquette, J. W. Scott, and S. W. Corzine, "Comprehensive numerical modeling of vertical-cavity surface-emitting lasers," *IEEE J. Quantum Electron.* **32**, pp. 607–616, 1996.
16. S. L. Chuang, "Efficient band structure calculations of strained quantum wells," *Phys. Rev. B* **43**, 1991.
17. I. Vurgaftman and J. R. Meyer, "Band parameters for III-V compound semiconductors and their alloys," *J. Appl. Phys.* **89**, pp. 5815–5875, 2001.
18. V. D. Kulakovskii, T. G. Andersson, and L. V. Butov, "Band edge offset in strained $\text{In}_x\text{Ga}_{1-x}\text{As}/\text{GaAs}$ quantum wells measured by high-excitation photoluminescence," *Semicond. Sci. Technol.* **8**, pp. 477–480, 1993.
19. C. F. Hsu, J. P. S. Zory, and C.-H. Wu, "Coulomb enhancement in InGaAs-GaAs quantum-well lasers," *IEEE J. Sel. Topics Quantum Electron.* **3**, 1997.
20. J. Piprek, D. Lasasosa, D. Pasquariello, and J. E. Bowers, "Optimization of GaAs amplification photodetectors for 700% quantum efficiency," *IEEE J. Sel. Topics Quantum Electron.* **9**, pp. 776–782, 2003.
21. M. Nawaz and K. Permthammasin, "A design analysis of a GaInP/GaInAs/GaAs-based 980 nm al-free pump laser using self-consistent numerical simulation," *Semicond. Sci. Technol.* **16**, pp. 877–884, 2001.
22. S. Seki, W. W. Lui, and K. Yokoyama *Appl. Phys. Lett.* **66**, pp. 3093–3095, 1995.
23. R. K. Ahrenkiel, R. Ellingson, and W. Metzger, "Auger recombination in heavily carbon-doped GaAs," *Appl. Phys. Lett.* **78**, pp. 1897–1881, 2001.
24. Y. Liu, W.-C. Ng, K. D. Choquette, and K. Hess, "Numerical investigation of self-heating effects of oxide-confined vertical-cavity surface-emitting lasers," *IEEE J. Quantum Electron.* **41**, pp. 15–25, 2005.
25. L. A. Coldren and S. W. Corzine, *Analysis and simulation of heterostructure devices*, Springer-Verlag Wien New York, Austria, 2004.
26. J. Piprek, T. Tröger, B. Schröter, J. Kolodzey, and C. S. Ih, "Thermal conductivity reduction in GaAs-AlAs distributed bragg reflectors," *IEEE Photon. Technol. Lett.* **10**, pp. 81–83, 1998.
27. R. Nagarajan, "Carrier transport effects in quantum well lasers: an overview," *Opt. Quantum Electron.* **26**, pp. S647–S666, 1994.
28. M. A. Alam, M. S. Hybertsen, R. K. Smith, and G. A. Baraff, "Simulation of semiconductor quantum well lasers," *IEEE T. Electron. Dev.* **47**, p. 1917, 2000.
29. H. W. Then, C. H. Wu, G. Walter, M. Feng, and N. Holonyak, "Electrical-optical signal mixing and multiplication ($2 \rightarrow 22\text{GHz}$) with a tunnel junction transistor laser," *Applied Physics Letters* **94**, p. 101114, 2009.
30. L. Zhang and J. P. Leburton, "Modeling of the transient characteristics of heterojunction bipolar transistor lasers," *IEEE Journal of Quantum Electronics* **45**, pp. 359–366, 2009.
31. M. Shirao, N. N. S. Lee, and S. Arai, "Large signal analysis of AlGaInAs/InP laser transistor," in *Conference on Lasers and Electro-Optics*, p. CMY7, (San Jose, CA), 2010.
32. A. Taflove and S. C. Hagness, *Computational electrodynamics: The finite-difference time-domain method*, Artech House, 2005.